DETECTING SURFACE MELT OF ANTARCTIC ICE-SHEETS USING SCATTEROMETERS

Lukas B. Kunz
Microwave Earth Remote Sensing Laboratory
Brigham Young University
Provo, UT 84602
PH: 801.422.4884 FAX: 801.422.6586
April 23, 2004

Abstract

The SeaWinds on QuikScat and ERS-1/2 scatterometers measure the radar response of the Earth's surface with high spatial- and temporal-resolution. The data collected by these space-borne active-microwave sensors are used to detect periods of surface melting in the Antarctic ice-shelves. A description of a statistical melt-detection algorithm is given and the results are shown and compared to other melt-detection methods.

SYMBOLS

σ^o = normalized radar backscatter coefficient
σ^o_H = horizontal polarization backscatter coefficient
σ^o_V = vertical polarization backscatter coefficient
PR = 'quasi' polarization ratio
T_b = brightness temperature (in Kelvins K)
HR = horizontal range of T_b
H_0 = null hypothesis
H_1 = alternative hypothesis
$f_{\mathbf{X}|H_0}(\mathbf{x}|h_0)$ = probability density function under H_0
$f_{\mathbf{X}|H_1}(\mathbf{x}|h_1)$ = probability density function under H_1
σ = standard deviation

INTRODUCTION

Accurate measurements of key characteristics of the polar ice-shelves are important to our understanding of the earth's climate. The extreme physical conditions of the polar regions make it very challenging and dangerous for humans to make these observations on site. Satellites provide a way to observe the entire earth without endangering lives and without using earth-bound weather stations.

Scatterometers are space-borne instruments that transmit pulses of microwave electromagnetic energy and measure the power reflected back to the sensor by the Earth's surface. This backscatter (σ^o) is heavily dependent upon how much liquid water is present on the surface. These measurements are particularly sensitive to the water content of the illuminated surface. Also, backscatter signatures observed from illuminating snow-covered ice and liquid water are markedly different.[1] As the amount of liquid water in the snow cover increases, the wet snow at the surface causes a dramatic decrease in the radar backscatter.[2] These changes in backscatter are used in an algorithm to determine the physical state of the surface of Antarctic ice-shelves. This algorithm is described in the next two sections.

Three different scatterometers are used in the study presented in this report. ERS 1 and ERS 2 were identical instruments that operated in C-band (5.3 GHz). Their missions provide data from 1992 to 2000. The SeaWinds on QuikScat scatterometer operates in Ku-band (13.6 GHz) and provides data from 1999 to present. The ERS sensors were on polar orbiting satellites that provided complete coverage of the polar regions every six days. The QuikScat instrument is able to completely cover the polar regions each day. Additionally, QuikScat measures the backscatter for both horizontal and vertical polarizations, σ^o_H and σ^o_V, respectively. ERS was only vertically polarized and provides measurements with significantly less resolution.

Many studies have been conducted using space-borne passive-microwave sensors to detect the surface melt of Arctic sea-ice.[3–5] However, the use of scatterometers in such studies is relatively limited[6] and their use in detecting surface melt in the Antarctic is even more limited.

Passive-microwave sensors record brightness temperature measurements, T_b. Several algorithms have been implemented on passive-microwave data to map snowmelt-onset dates on Arctic sea-ice.[6] A similar algorithm is used in this paper in order to validate the melt detection results from the scatterometer measurements. The SSM/I passive-microwave sensor is onboard one of the Defense Meteorological Satellite Program (DMSP) satellites and provides observations at four frequencies: dual-polarization at 19.35, 37.0, and 85.5 GHz, and 'v-pol' at 22.235 GHz. High-resolution images of the measurements from QuikScat and the SSM/I sensors produced using the Scatterometer Image Recon-

struction (SIR) algorithm[7] are used in the analysis presented.

An initial algorithm for determining a backscatter threshold to use for melt detection is presented. This is shown to be inadequate. A maximum likelihood (ML) approach is then taken to determine daily ice-state classifications from the scatterometer backscatter measurements. These ice-state estimates are strongly correlated with the melt-detection results from passive-microwave data and give added insight due to the higher spatial-resolution and increased sensitivity achieved by the active-microwave scatterometer instruments.

INITIAL THRESHOLD DETECTION

Ideally, a natural threshold would exist that determines a melting event. In order to discover if this threshold exists the following method is used. First, for each year spanned by the available data the mean winter backscatter value for each location is computed. Then, each day during the non-winter months that the backscatter value drops below the winter mean value by more than the threshold is counted as a melt event for the given location. The number of total melt events during each year is multiplied by the spatial resolution of the sensor to calculate the cumulative melt area. This process is repeated for various threshold values. To constrain the analysis to the ice-shelves only, a spatial mask is applied to the data. Figure 1 shows the regions that are used in the algorithm. Sea-ice and high-elevation areas are excluded.

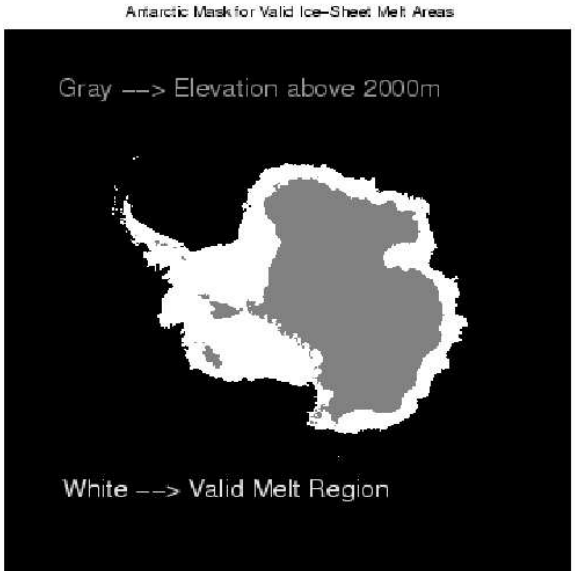

Figure 1: The valid region for the melt detection algorithm. Locations above 2000m in elevation are excluded. It is assumed no melting occurs there. Sea-ice is excluded due to its changing daily location.

This method is applied to the ERS-1/2 σ^o_V and QuikScat σ^o_H datasets. For the ERS sensors, the threshold is varied from 0.25 dB to 6.0 dB. The thresholds for the QuikScat data range from 1.0 dB to 6.0 dB. Figures 2 and 3 show the results of the melt detection. The amount of melt is consistent between the two sensors, but no natural threshold appears. Even though the amount of detected melt is similar for thresholds between 3 dB and 6 dB, there is still too large of a discrepancy to confidently select one of these thresholds to use in a melt-detection algorithm.

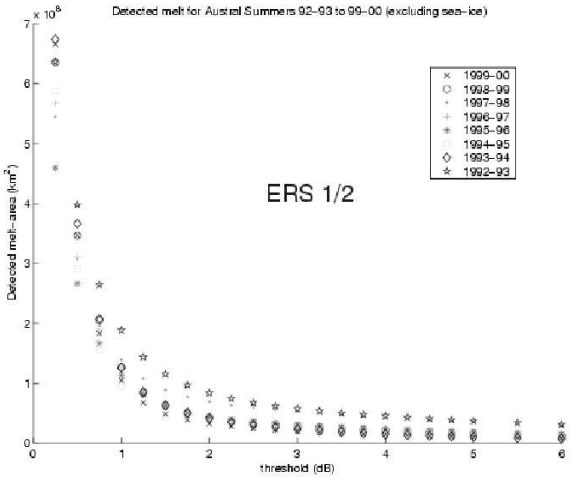

Figure 2: Cumulative melt-area vs. threshold for the ERS-1/2 missions. The exponential curve suggests that no reliable natural threshold exists for use in melt detection.

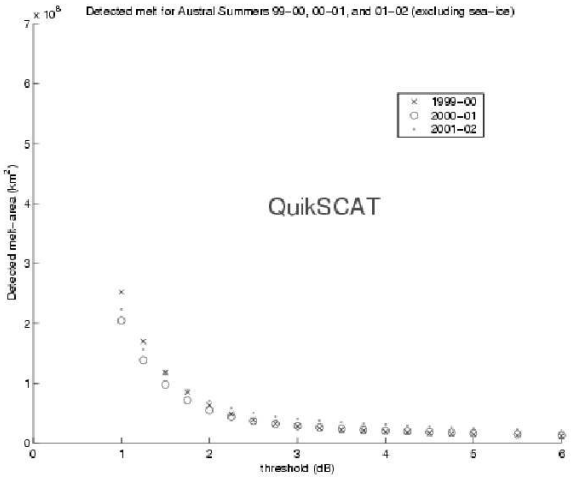

Figure 3: Cumulative melt-area vs. threshold for QuikScat data. These results are consistent with the ERS results and yield no ideal threshold value.

MAXIMUM LIKELIHOOD DETECTION

The simple algorithm previously presented used only one backscatter polarization for each sensor. This is all the data available from ERS-1/2, so a significant improvement in melt-detection using such measurements can not be expected. The QuikScat scatterometer, however, measures dual-polarization backscatter (σ^o_H and σ^o_V). These values are very correlated but do exhibit different sensitivities to the presence of liquid water. This additional information leads to the improved melt-detection algorithm presented in this section.

For QuikScat the v-pol backscatter response tends to be less reactive to changing water content than the h-pol response. This difference in sensitivity is accentuated by using the 'quasi' polarization ratio (PR) defined by

$$PR = \sigma^o_V - \sigma^o_H, \tag{1}$$

where the values are in dB. This is not a true polarization ratio since the two polarizations are at different incidence angles. The h-pol beam is at a nominal incidence angle of $\sim 46°$ while the v-pol beam is at $\sim 54°$. The σ^o_V value is generally $\sim$2dB below the typical σ^o_H measurement.

The time-series of the h-pol and PR values from a selected point on the Shackleton Ice-shelf is shown in Figure 4. Observing these values from 1999 through 2003 reveals that during each Austral summer the PR actually becomes positive due to the greater sensitivity of the h-pol measurements to liquid water in the ice-shelf surface snowcover. This time-series is typical of most areas that experience surface melting while the backscatter values for locations with no melt events are nearly constant.

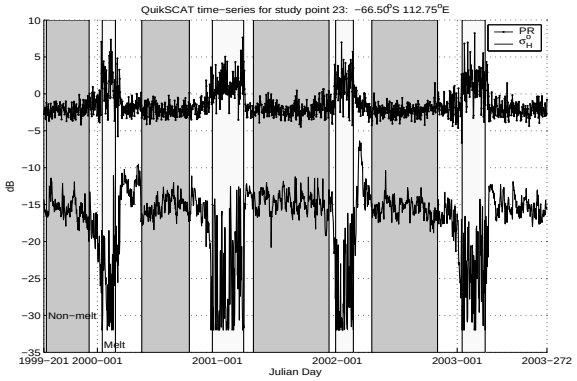

Figure 4: σ^o_H and PR time-series for a selected point on the Shackleton Ice-shelf. During each year contiguous periods of alternating melt and non-melt are identified. Each period's mean and covariance are found empirically and used in maximum likelihood estimations of the daily ice-states.

Figure 5 contains scatterplots for each year of σ^o_H vs. PR for this same location. Note the high concentration of values around the point (-15dB,-2dB) in each plot and the loose grouping of the remaining points. This suggests that the backscatter and PR observations may be modeled as random variables with some mean and covariance. An explanation of the method used to compute the distributions of these random variables is presented. Afterwhich the procedure for estimating the physical state of the local surface-ice for each day is discussed.

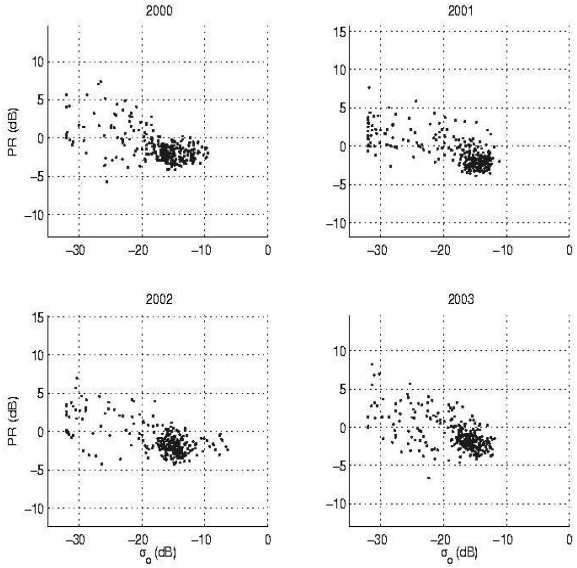

Figure 5: Yearly scatterplots of σ^o_H vs. PR for Shackelton Ice-shelf location.

Ice-state Distribution Estimations

To observe the intra- and inter-shelf radar response characteristics 25 study points are selected from each of the major ice-shelves (Figure 6). It is assumed that the backscatter and PR values are jointly gaussian for solid ice or liquid water. Figure 4 also indicates the periods used to empirically calculate the mean and covariance for each year's melting and non-melting conditions. These values completely specify the gaussian distribution governing the proposed model.

Figure 7 shows the resulting 1-σ contours for each year's melt and non-melt periods. These contours match well with the groupings of values on the scatterplot in Figure 5. It is important to note that the distributions do not change significantly from year to year for this location. Most of the other selected study points also exhibit this behavior. Figure 8 shows the distributions for this location using all values from a neighborhood of radius 20km. The distribution changes very little by including the measurements from the surrounding area.

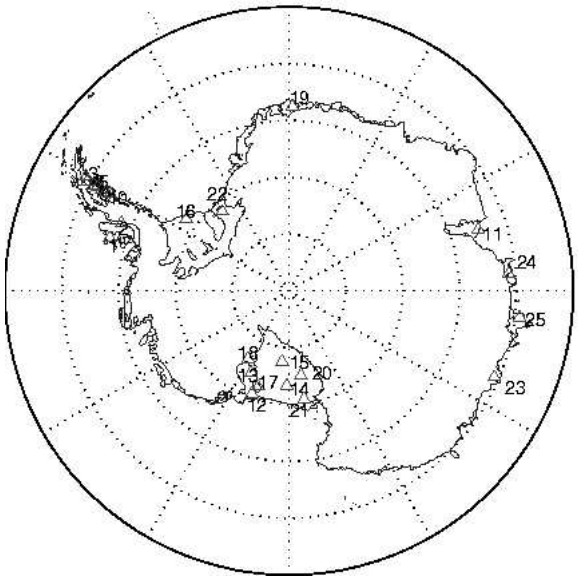

Figure 6: The 25 selected study points over Antarctic ice-shelves.

These results, coupled with observing the distributions of the other selected study points, indicate that the non-melt and melt distributions are approximately temporally- and spatially-invariant within a given ice-shelf. In general, this invariance property does not hold for locations near ice-shelf boundaries.

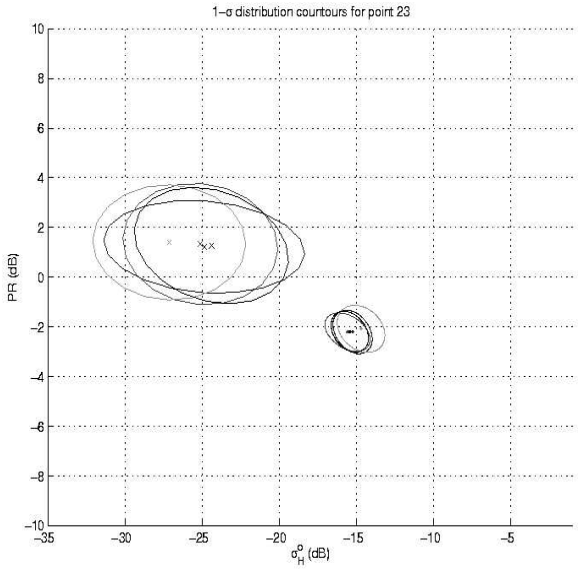

Figure 7: Yearly bivariate normal distribution 1-σ covariance contours for study point 23. The mean values for each period are indicated by an 'x' or a dot at the middle of the respective contour.

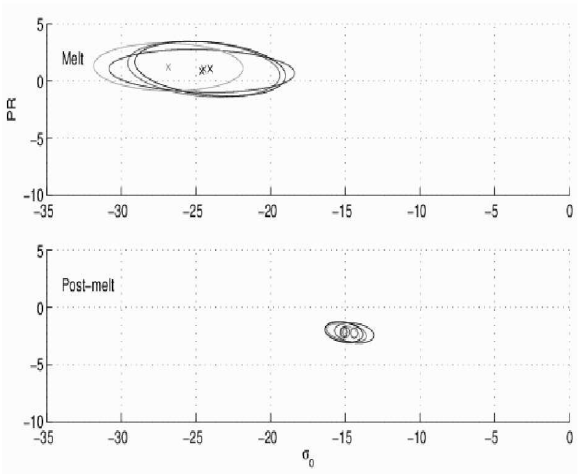

Figure 8: Yearly distribution contours for a 9-pixel (20km) radius neighborhood of study point 23.

ML Estimation of Ice-states

To use the maximum likelihood method to select the daily ice-state for each location the binary hypothesis test is formed

$$H_0: \ \mathbf{X} \sim \mathcal{N}(\mathbf{m_0}, \mathbf{R_0})$$
$$H_1: \ \mathbf{X} \sim \mathcal{N}(\mathbf{m_1}, \mathbf{R_1})$$

where H_0 denotes the conditions for no surface melting and H_1 represents the presence of surface melt. $\mathbf{X}$ is a two-element vector in the space spanned by the possible values of σ^o_H and PR, $\mathbf{m_o}$ and $\mathbf{m_1}$ contain the estimated mean σ^o_H and PR values for each ice-state. R_0 and R_1 are the respective covariance matrices.

The likelihood ratio

$$l(x) = \frac{f_{\mathbf{X}|H_1}(\mathbf{x}|h_1)}{f_{\mathbf{X}|H_0}(\mathbf{x}|h_0)} > \frac{L_{01}P(H_0)}{L_{10}P(H_1)} \qquad (2)$$

is the basis for the maximum likelihood test, where L_{ij} is the loss associated with choosing ice-state j when the true state of nature is i, and $P(H_i)$ is the prior probability that ice-state i is the true situation. The maximum likelihood approach assumes no $a\ priori$ information so equal losses and prior probabilities are chosen.

Forming the log-likelihood ratio $\Lambda(\mathbf{x}) = \log l(\mathbf{x})$ simplifies the hypothesis test to

$$\phi(\mathbf{x}) = \begin{cases} 1 & \|\mathbf{x}-\mathbf{m_1}\|_{\mathbf{R_1}^{-1}} < \|\mathbf{x}-\mathbf{m_0}\|_{\mathbf{R_0}^{-1}} + \log\frac{|\mathbf{R_0}|}{|\mathbf{R_1}|} \\ 0 & \text{otherwise} \end{cases} \qquad (3)$$

where

$$\|\mathbf{x}-\mathbf{m_i}\|_{\mathbf{R_i}^{-1}} \stackrel{\triangle}{=} (\mathbf{x}-\mathbf{m_i})^H \mathbf{R_i}^{-1}(\mathbf{x}-\mathbf{m_i}). \qquad (4)$$

This maximum likelihood test is performed for each of the 25 study points over the span of the entire data set. For each year the respective mean $\mathbf{m_i}$ and covariance $\mathbf{R_i}$ are used in the estimation. Figure 9 shows the resulting maximum likelihood estimates of the ice-state for each day at the same location as in the previous figures.

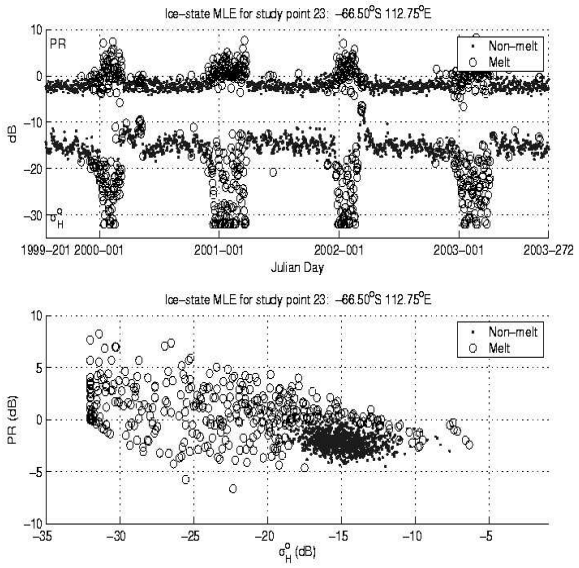

Figure 9: Time-series and scatterplot for study point 23 with resulting ML method surface-melt estimates.

This algorithm appears to perform quite well because it properly determines cases of obvious surface melt marked by drastically decreasing backscatter values and positive PR values. Some days are selected as melting events, however, that are not marked by significant changes in the time-series values. The results from a location on the Ross Ice-shelf are given in Figure 10. The ML method results in no classified melt events. This is expected since this shelf is extremely stable and rarely experiences any significant melting. Figure 11 shows the results for a point on the Fimbul Ice-shelf. This location experiences substantial melting. Note the unusual behavior of the measurements during 2003. Even though the backscatter actually increased during the Austral summer of this year the ML melt-detection method still identifies many melt events. In order to validate the melt-detection classifications yielded by the ML approach, data from a passive-microwave instrument is analyzed.

VALIDATION USING RADIOMETER DATA

Passive-microwave brightness temperature measurements have been used to detect melt on Arctic sea-ice using the SSM/I sensor. The horizontal range, defined by $HR = T_b(19H) - T_b(37H)$, is used to determine if a melting event has occurred.[6] If this value drops below $2K$ a melt event is counted. Although this method was only applied to Arctic sea-ice, it is assumed that the brightness temperatures of Antarctic shelf-ice are also valid for this application.

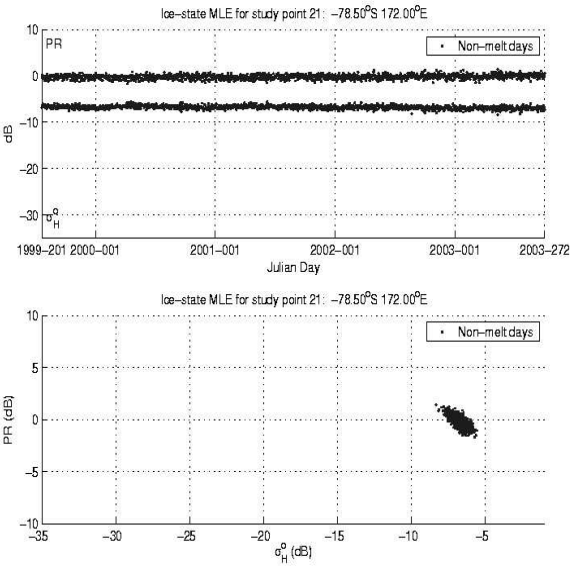

Figure 10: Time-series and scatterplot for study point 21 with resulting ML method surface-melt estimates.

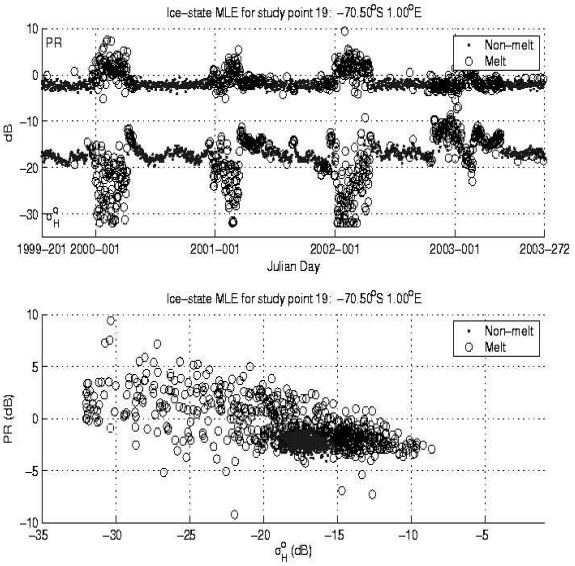

Figure 11: Time-series and scatterplot for study point 19 with resulting ML method surface-melt estimates.

The lower portions of Figures 12-14 show the time-series of available SSM/I data corresponding to the QuikScat dataset for two locations. Note the similar behavior of the measurements from both instruments when melt is detected by both sensors. Figure 13 reveals that

for the Ross Ice-shelf location (point 21) the measured backscatter is nearly constant while the T_b values vary considerably. Passive-microwave observations are more subject to changing atmospheric conditions. This may explain the discrepancy between the two sensors for this location. The variation in responses between the SSM/I channels are due to the different operating frequencies and polarizations. Higher-frequency channels are effected more by atmospheric opacity.

The results of the HR-based melt-detection algorithm are shown in the upper portions of these figures as dots along the bottom of the plot. For study point 23 the SSM/I measurements result in a significantly higher number of melt events than for QuikScat. This is reversed for study point 19.

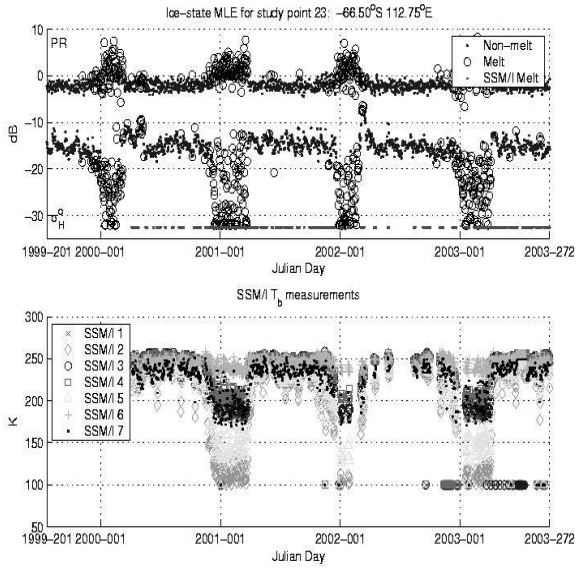

Figure 12: Combined results from the ML method for QuikScat and the HR method using SSM/I data for point 23. The HR method classifies many days as melt events that the ML method does not. The HR classifications are indicated at the bottom of the QuikScat time-series as a single dot for each day of melt.

CONCLUSIONS

The active-microwave scatterometers are less susceptible to atmospheric interference than their passive-microwave counterparts. This is a great advantage in determining the surface characteristics of Antarctic ice-shelves since much of this region is storm-ridden for most of the year. It was shown that the initial threshold method was inadequate for properly determining melt events on the ice-shelves. Consequently, the ERS-1/2 datasets appear to offer less than desirable observations for this application. The maximum likelihood melt-detection algorithm using

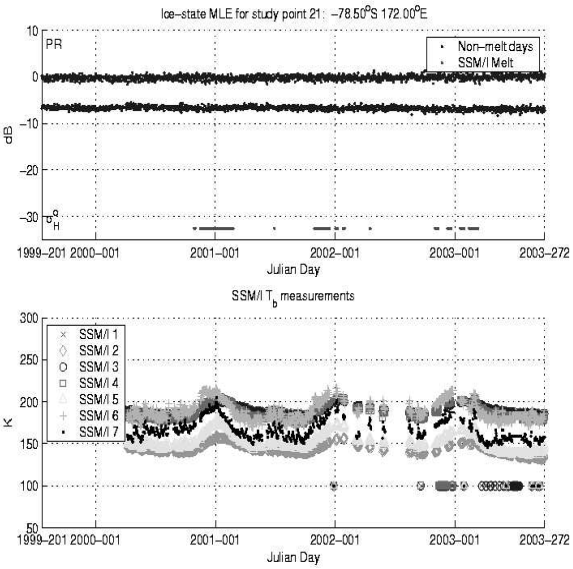

Figure 13: Combined results from the ML method for QuikScat and the HR method using SSM/I data for point 21. The HR method classifies some days as melt events while QuikScat shows no significant changes in its backscatter values. No actual melting is expected to have taken place.

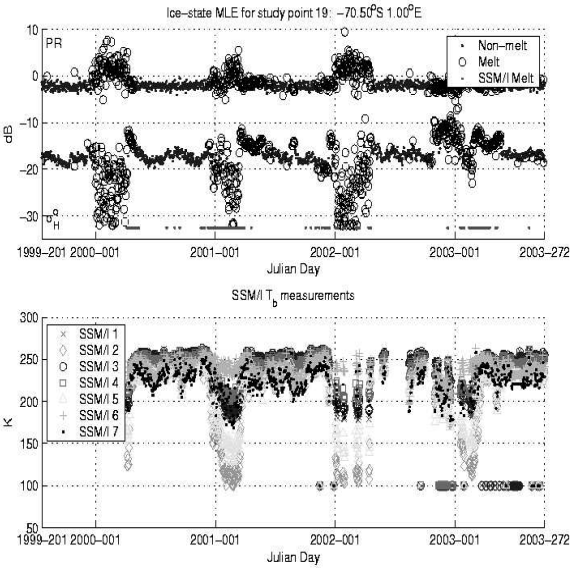

Figure 14: Combined results from the ML method for QuikScat and the HR method using SSM/I data for point 19. In this case the HR method classifies fewer days as melt events than the ML method.

QuikScat dual-polarization measurements was shown to be a promising method for detecting surface melting.

The validation of the QuikScat results consisted of implementing a passive-microwave method previously used for Arctic sea-ice melt-detection. Comparing the two methods reveals that using QuikScat measurements is very effective in determining the presence of surface melting on Antarctic ice-shelves. The results are consistent with the SSM/I observations. Additionally, the backscatter observed by QuikScat is at a much finer resolution (2.25km/pixel for SIR images) than the T_b measurements (8.9km/pixel for SIR images). This allows for more precise observation of spatially-varying surface-melt. Future work on this subject involves creating maps of the melt-onset and refreeze dates for each major ice-shelf.

References

[1] Frank D. Carsey, *Microwave Remote Sensing of Sea Ice*, American Geophysical Union, Washington, D.C., 1992.

[2] F.T. Ulaby, R.K. Moore, and A.K. Fung, *Microwave remote sensing, active and passive. Vol. 2. Radar remote sensing and surface scattering and emission theory*, Addison-Wesley Publishing Co., Reading, MA, 1982.

[3] W.J. Campbell, P. Gloersen, and H.J. Zwally, "Aspects of arctic sea ice observable by sequential passive-microwave observations from the Nimbus 5 satellite", in *Arctic Technology and Policy*, C. Chryssostomidis I. Dyer, Ed., pp. 197–222. Hemisphere Publishing, New York, 1984.

[4] M.R. Anderson, "The onset of spring melt in first-year ice regions of the arctic as determined from SMMR data for 1979 and 1980", *Journal of Geophysical Research*, vol. 92(C12): 13,153-13,163.

[5] K. Garrity, "Characterization of snow on floating ice and case studies of brightness temperature change during the onset of melt", in *Microwave remote sensing of sea ice*, F.D. Carsey and 7 others, Eds., 68, pp. 313–328. American Geophysical Union, Washington, D.C., 1992.

[6] R.R. Forster, D.G. Long, K.C. Jezek, S.D. Drobot, and M.R. Anderson, "The onset of arctic sea-ice snowmelt as detected with passive- and active-microwave remote sensing", *Annals of Glaciology*, vol. 33.

[7] David G. Long and D. Daum, "Spatial resolution enhancement of SSM/I data", *IEEE Trans. Geosci. Remote Sensing*, vol. 36, pp. 407–417.